RSC Advances

PAPER

View Article Online
View Journal | View Issue

Cite this: *RSC Adv.*, 2023, **13**, 7037

Ru-based monolithic catalysts for the catalytic oxidation of chlorinated volatile organic compounds†

Yemin Zhao,[abd] Chao Xi,[bd] Shan Gao,*[bd] Yuejun Wang,[bd] Haiqiang Wang,[ad] Pengfei Sun[c] and Zhongbiao Wu[ad]

Received 8th December 2022
Accepted 16th February 2023

DOI: 10.1039/d2ra07823f

rsc.li/rsc-advances

A series of cordierite monolithic catalysts with Ru species supported on different available low-cost carriers were prepared and investigated for the elimination of CVOCs. The results suggest that the monolithic catalyst with Ru species supported on anatase TiO_2 carrier with abundant acidic sites exhibited the desired catalytic activity for DCM oxidation with the $T_{90\%}$ value of 368 °C. In addition, a pseudo-boehmite sol used as binder was introduced into the preparation of the monolithic catalysts to further improve the adhesion between the powder catalysts and cordierite honeycomb carrier. The results suggest that although the $T_{50\%}$ and $T_{90\%}$ of the Ru/TiO_2/PB/Cor shifted to higher temperature of 376 and 428 °C, the weight loss of the coating for the Ru/TiO_2/PB/Cor catalyst was improved and decreased to 6.5 wt%. Also, the as-obtained Ru/TiO_2/PB/Cor catalyst exhibited ideal catalytic properties for the abatement of ethyl acetate and ethanol, indicating that the catalyst can meet the demand for the treatment of actual multi-component industrial gas.

1. Introduction

Chlorinated volatile organic compounds (CVOCs) such as dichloromethane (DCM), chlorobenzene (CB) and 1,2-dichloroethane (DCE) are widely utilized in the production processes of pharmaceuticals, synthetic resins, adhesives and coatings, and printing.[1–4] Nevertheless, most CVOCs are considered as hazardous pollutants due to their severe toxicity and persistent threat to humans and the environment. Therefore, eliminating CVOC pollutants from the atmosphere becomes more urgent in order to protect the environment and promote harmonious relationships between humans and nature.[5,6]

Among the advanced treatment technologies, catalytic oxidation, which converts chlorinated compounds into the desirable products of H_2O, CO_2 and HCl, has been in focus because they have the advantages of high conversion efficiency, moderate operation temperature and low energy consumption.[7–9] Over the past decades, much effort has been made to improve the catalytic oxidation of CVOCs through development of efficient catalysts for the conversion process. Among the various catalytic materials, transition metal oxides, such as CeO_2, MnO_x, TiO_2, ZrO_2–TiO_2, have been prepared in various strategies and investigated by modulating their reducibility, surface acidity, structure and morphology.[10–17] For example, Zhan *et al.* prepared a series of Mn–Ti composite oxides with different surface acidity and reducibility through adjusting the Mn/Ti molar ratio, they found the catalyst surface acidity had an important effect on the oxidation of vinyl chloride.[7] Zhou *et al.* synthesized several CeO_2–ZrO_2–CrO_x mixed oxides and found the introduction of Zr^{4+} into the CeO_2–CrO_x can improve the catalytic oxidation of 1,2-dichloroethane remarkably since the ZrO_2 doping was considered to raise the amount of the Cr^{6+} species and oxygen vacancies of the catalysts.[13] Although the transition metal oxides exhibit superior catalytic performance, they are susceptible to inorganic chlorine species, which probably results in the quickly deactivation of the catalysts. Noble metal catalysts, such as Pt, Pd and Ru, have also attracted considerable attention in exploring their catalytic performance over the CVOCs conversion.[18–28] Previous studies have indicated that Ru-based catalysts produce less polychlorinated by-products since the Cl species can be removed rapidly from the surface in form of Cl_2 through the Deacon reaction in comparison with Pd and Pt-based materials. Zeolite catalysts with high specific surface area, outstanding thermal stability, intricate channels are also widely applied in CVOCs catalytic oxidation.[29–33] Unfortunately, coke deposition

[a]*Department of Environmental Engineering, Zhejiang University, Hangzhou 310058, P. R. China*

[b]*Zhejiang Tianlan Environmental Protection Technology Co., Ltd., Hangzhou 311202, China. E-mail: gaoshan@tianlan.cn*

[c]*Department of Chemistry, Key Laboratory of Surface & Interface Science of Polymer Materials of Zhejiang Province, Zhejiang Sci-Tech University, Hangzhou 310018, China*

[d]*Zhejiang Provincial Engineering Research Center of Industrial Boiler & Furnace Flue Gas Pollution Control, 866 Yuhangtang Road, Hangzhou 310058, P. R. China*

† Electronic supplementary information (ESI) available. See DOI: https://doi.org/10.1039/d2ra07823f

and chlorine poisoning on zeolites surface can lead to the deactivation of catalytic performance rapidly.

In addition, the catalytic activities of noble metal supported catalysts are associated with various carriers.[24] Recently, Ying and co-workers explored the catalytic oxidation of DCM over Ru-based materials with different carriers (Al_2O_3, TiO_2, HZSM-5 $SiO_2/Al_2O_3 = 27$ and 130), and they found that the Lewis acid sites on surface of carriers were more active for the C–Cl cleavage in comparison with Brønsted acid sites. Additionally, the Cl species deposited on the Al_2O_3 and TiO_2 were more prone to generate polychlorinated by-products especially the dibenzo-*p*-dioxins and dibenzofurans (PCDD/Fs) through the electrophilic chlorination reactions.[34]

On the other hand, previous mechanism studies have indicated that the surface acidity of the catalyst affect the catalytic oxidation of CVOCs. Because the adsorption and the breakage of C–Cl bonds usually occurred on the carriers with abundant acid sites on their surface, such as TiO_2.[30] In addition, for Ru-based catalysts, the dissociated Cl species will be rapidly transferred to the Ru species from the active sites, and followed by the generation of Cl_2 through Deacon reaction.[20,34]

Monolithic catalysts have been intensively developed and used in various practical industrial applications for effective abatement of the polluted waste gas such as VOCs and NO_x due to their lower pressure drop, higher mechanical strength and superior heat and mass transfer property in comparison with conventional powder catalysts and granular catalysts.[35–39] Cordierite honeycomb ($2MgO \cdot 2Al_2O_3 \cdot 5SiO_2$) is a common monolithic catalysts substrate with low cost and abundant resource, and has been explored for catalytic oxidation of non-chlorine VOCs, such as ethyl acetate, methane and toluene.[40–42] For example, Ren *et al.* fabricated a series of $M_xCo_{3-x}O_4$ (M = Zn, Ni, Co) nanoarray materials that supported on cordierite monolithic substrates through *in situ* hydrothermal synthesis for methane and carbon monoxide catalytic oxidation reaction, however, their hydrothermal approach of monolithic catalysts was time-consuming and complicated, which made it difficult for scalable fabrication.[43] In general, over the past years, although catalysts with various active components and structures have been intensively synthesized and displays ideal catalytic activity and stability for the catalytic degradation of CVOCs, most of these reported catalysts are powdery, and few literature related to the performance of monolithic catalysts have been reported probably due to the complexity of preparation of catalysts and coating slurry as well as the high requirement for testing device, especially for its resistance to chlorine corrosion.[15,42] Therefore, adopting feasible and facile methods to prepare catalysts and support them on monolithic substrate as well as studying their catalytic performance in fixed-bed reactor made by chlorine corrosion resistance alloy in a more applicable perspective become urgently, which may be beneficial for the guide of future pilot test or engineering applications.

Consequently, in this work, cordierite monolithic catalysts with Ru species supported on different low-cost available carriers (TiO_2, P25, CeO_2) are prepared through coating the powder catalysts on cordierite honeycomb monoliths and investigated their catalytic activity toward dichloromethane catalytic oxidation. On the other hand, as previous study indicates that the low-cost all-silicon beta zeolite supported Pt catalyst (Pt/Si-beta) showed the best catalytic activity for the catalytic combustion of methylcyclohexane due to its superior hydrocarbon adsorption capacity and hydrophobicity compared to the all-silicon ZSM supported Pt and SBA-15 supported Pt catalysts.[44] Thus, monolithic catalyst with Ru species loaded on all-silicon beta zeolite is also explored. In addition, the properties of these as-prepared catalysts were further examined by N_2 adsorption–desorption, XRD, XPS, NH_3-TPD techniques, respectively. Here, the DCM was chosen as a reactant to investigate the catalytic activity of the catalysts. We believe that our work is capable of providing deep insight into designing and preparing monolithic catalysts for efficient catalytic oxidation not only for CVOCs but also for multicomponent VOCs that intensively exists in industrial exhausts from a more practical point of view.

2. Experimental

All chemicals are commercials available (Table 1).

2.1 Catalyst preparation

2.1.1 Preparation of Ru/TiO_2 catalyst powder. First, thirty grams of TiO_2 was dispersed in the deionized water (200 mL), then 0.81 g $RuCl_3 \cdot nH_2O$ (Ru content: 37 wt%, Kunming Boren Precious Metal Co., LTD) was added into the suspension. After stirring for 2 h, the mixture was dried at 120 °C for overnight, and calcined at 450 °C for 3 h in the muffle furnace to afford the final catalyst powder. The obtained catalyst powder denoted as Ru/TiO_2, and the mass ration of Ru to TiO_2 was about 1.0%.

2.1.2 Preparation of Ru/P25, Ru/Si-beta and Ru/CeO_2 catalysts powder. The preparation procedure of Ru/P25, Ru/Si-beta and Ru/CeO_2 was similar to that of Ru/TiO_2 by replacing TiO_2 with P25, Si-beta and CeO_2, respectively.

2.1.3 Preparation of Ru/TiO_2/Cor catalyst. The as-obtained Ru/TiO_2 catalyst powder (15 g) was added into the deionized water (100 g), and the mixture was ball-milled at 500 rpm for 30 min to afford homogeneous slurry. Subsequently, cordierite (Cor) honeycomb monolith (200 cpsi, 22 mm × 22 mm × 50 mm, ~12.5 g) was immersed in the as-obtained slurry directly for thirty seconds. After that, the excess slurry in pores was removed by compressed air, and the coated catalyst was dried at 120 °C for 3 h, followed by calcination at 450 °C in air for 3 h. The coating procedure was repeated to achieve the desired catalyst loading of 12.5 ± 0.5 wt% (mass of catalyst: ~1.6 g), based on the weight after calculation. Finally, the monolithic catalyst was achieved and marked as Ru/TiO_2/Cor. The loading was calculated by using the following equation:

$$\text{Loading (wt\%)} = \frac{M_1 - M_0}{M_0} \times 100\%$$

where M_0 is the mass of pristine cordierite honeycomb monolith; M_1 is the mass of the monolithic catalyst after coating and calcination.

Table 1 The sources of carriers

Chemicals	Source	Purity
All-silicon beta zeolite (Si-beta)	Zhejiang Taide New Material Co., Ltd	≥90%
Anatase titanium dioxide (TiO_2)	Sichuan Huatie Vanadium and Titanium Technology Co., Ltd	≥97%
Cerium dioxide (CeO_2)	Yutai Qingda Fine Chemical Co., Ltd	≥99%
P25	Degussa Co., Ltd	AR

2.1.4 Preparation of Ru/P25/Cor, Ru/Si-beta/Cor and Ru/CeO_2/Cor catalysts. The Ru/P25/Cor, Ru/Si-beta/Cor and Ru/CeO_2/Cor catalysts were prepared in a similar procedure for preparing Ru/TiO_2/Cor by replacing Ru/TiO_2 catalyst powder with Ru/P25, Ru/Si-beta and Ru/CeO_2 catalysts powder, respectively.

2.1.5 Preparation of TiO_2/Cor. The preparation procedure of TiO_2/Cor was similar to that of Ru/TiO_2/Cor by replacing Ru/TiO_2 with TiO_2.

2.1.6 Preparation of Ru/TiO_2/PB/Cor. Pseudo-boehmite (0.75 g) and 8.75 wt% nitric acid (0.3 g) were added into the deionized water (100 g), and the mixture was stirred for 30 min. Then the as-obtained Ru/TiO_2 catalyst powder (15 g) was added into the above mixture, and followed by ball-milling at 500 rpm for 30 min to afford homogeneous slurry. Subsequently, cordierite honeycomb monolith was immersed in the as-obtained slurry directly for thirty seconds. After that, the excess slurry in pores was removed by compressed air, and the coated catalyst was dried at 120 °C for 3 h, followed by calcination at 450 °C in air for 3 h. The coating procedure was repeated to achieve the desired catalyst loading of 12.5 ± 0.5 wt% (mass of catalyst: ~1.6 g), based on the weight after calculation. Finally, the monolithic catalyst was achieved and marked as Ru/TiO_2/PB/Cor.

2.1.7 Preparation of Ru/P25/PB/Cor, Ru/Si-beta/PB/Cor and Ru/CeO_2/PB/Cor catalysts. Ru/P25/PB/Cor, Ru/Si-beta/PB/Cor and Ru/CeO_2/PB/Cor catalysts were prepared in a similar procedure for preparing Ru/TiO_2/PB/Cor by replacing Ru/TiO_2 catalyst powder with Ru/P25, Ru/Si-beta and Ru/CeO_2 catalysts powder.

2.2 Catalyst characterization

XRD patterns were recorded on an X-ray powder diffractometer (Bruker D8 ADVANCE A25X). X-ray photoelectron spectroscopy (XPS) of the catalysts was probed on a Thermo Fisher Scientific K-Alpha instrument with a monochromatic Al Kα X-ray source ($h\nu = 1486.8$ eV). All of the binding energies were referenced to the C 1s peak (284.8 eV) corresponding to adventitious carbon. NH_3-Temperature Programmed Desorption (NH_3-TPD) of samples were examined in Tianjin Xianquan Industry and Trade Development Co. Ltd. Typically, 100 mg sample was pretreated in pure He at 400 °C for 1 h, then the sample was saturated with 4% NH_3 in He (30 mL min^{-1}) at 30 °C for 30 min and subsequently heated to 100 °C. Thereafter, the sample was heated at a rate of 10 °C min^{-1} in pure He to desorb the NH_3. The weight loss of coating on monolithic catalysts is evaluated by ultrasonic vibration. Typically, the monolithic catalyst was placed in an ultrasonic bath for 30 min, and the sample was then washed by deionized water and dried at 120 °C for 3 h and weighed.

$$\text{Weight loss of coating (wt\%)} = \frac{M_1 - M_2}{M_1 - M_0} \times 100\%$$

where M_0 is the mass of pristine cordierite honeycomb monolith; M_1 is the mass of the monolithic catalyst after coating and calcination; M_2 is the mass of the monolithic catalyst after ultrasonic vibration and dry.

2.3 Catalytic activity evaluation

The dichloromethane, ethyl acetate (EA) and ethanol (EtOH) catalytic activities of as-prepared monolithic catalysts were tested in a conventional fixed-bed reactor, and the monolithic catalysts were placed in the constant temperature zone of the reactor. The reactor was continuously heated and the temperature of the reactor was maintained at the set temperature before analysing the VOCs concentration. The gaseous reactants (DCM, EA and EtOH) were generated by air stream through the liquid reactants in a saturator, and then diluted by another air stream. Here, the indoor air without any purification was used. The liquid reactants were maintained at 0 °C in an ice-water bath during the experiments, respectively. The mass flow controllers (Sevenstar Electronics) were applied to regulate the air intake flow. The total flow was about 6.05 L min^{-1} and the gas hourly space velocity (GHSV) was kept at 15 000 h^{-1} with an initial gaseous reactant concentration of about 1000 ppm that was tested at 250 °C in inlet. The DCM concentration in both inlet and outlet of the reactor was monitored by the gas chromatograph (Fuli, China) with flame ionization detector (FID). The schematic diagram of experimental set-up is displayed in Fig. S1.† Additionally, the ethyl acetate and ethanol concentration in both inlet and outlet of reactor was analyzed by the EXPEC 3200 portable gas chromatograph (Hangzhou PuYu Technology Development Co., Ltd. China) with flame ionization detector. The CO_2 was analysed by the GC with a Ni convertor furnace. The DCM conversion (%) and CO_2 yield (%) were calculated by using the following equation:

$$\text{DCM conversion (\%)} = \frac{[\text{DCM}]_{in} - [\text{DCM}]_{out}}{[\text{DCM}]_{in}} \times 100\%$$

where $[DCM]_{in}$ denotes the DCM concentration in the inlet gas. $[DCM]_{out}$ denotes the DCM concentration in the outlet gas.

$$CO_2 \text{ yield (\%)} = \frac{[CO_2]_{out} - [CO_2]_{in}}{[\text{DCM}]_{in}} \times 100\%$$

where $[CO_2]_{in}$ is the CO_2 concentration in the inlet. $[CO_2]_{out}$ is the CO_2 concentration in the outlet. $[DCM]_{in}$ is the DCM concentration in the inlet gas.

3. Results and discussion

Fig. 1 displays the preparation strategy for the formation of the monolithic catalyst. The cordierite honeycomb was immersed in the slurry containing the powder catalyst after ball milling for several minutes, then the excess slurry in pores was removed by compressed air, and the coated catalysts was dried and further subjected to calcination in air to obtain the monolithic catalyst. The powder X-ray diffraction (XRD) patterns of the various samples are shown in Fig. 2. For the Ru/TiO_2 catalysts, the diffraction peaks located at 25.3°, 37.8° and 48.1° can be attributed to the (101), (004) and (200) planes of anatase TiO_2 (PDF #21-1272).[20,45] As for Ru/P25 catalyst, the peaks of rutile TiO_2 phase at 27.5° and 36.1° are also observed and can be indexed to the (110) and (101) lattice plane of rutile TiO_2 (PDF #21-1276), suggesting the existence of rutile and anatase binary titanium dioxide in Ru/P25 catalyst.[34] The characteristic peak at 21.5° and 22.5° of Si-beta zeolite are observed over the Ru/Si-beta catalyst. Diffraction peaks at 28.6°, 33.1°, 47.5° and 56.3° can be observed on Ru/CeO_2 catalyst ascribing to the (111), (200), (220) and (311) planes of CeO_2 (PDF #34-0394), respectively.[13] Additionally, the peaks at 27.9° and 35.0° corresponding to the (110) and (101) planes of RuO_2 (PDF #43-1027) can be found in Ru/TiO_2 and Ru/Si-beta, respectively.[20,28] No obvious diffraction peaks from Ru species in Ru/CeO_2 and Ru/P25, probably owing to better dispersion in these catalysts. In addition, as shown in Fig. S2,† Ru/TiO_2/PB/Cor monolithic catalyst displays the characteristic peaks of anatase TiO_2 and cordierite

Fig. 1 Preparation route for the monolithic catalyst.

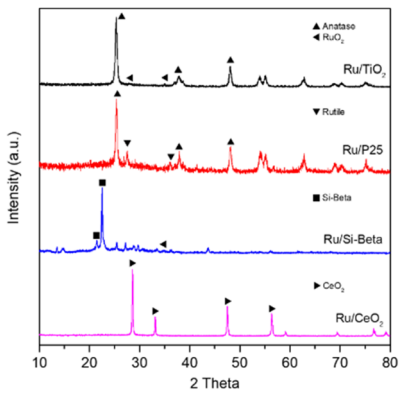

Fig. 2 The XRD patterns of Ru/TiO_2, Ru/P25, Ru/Si-beta and Ru/CeO_2.

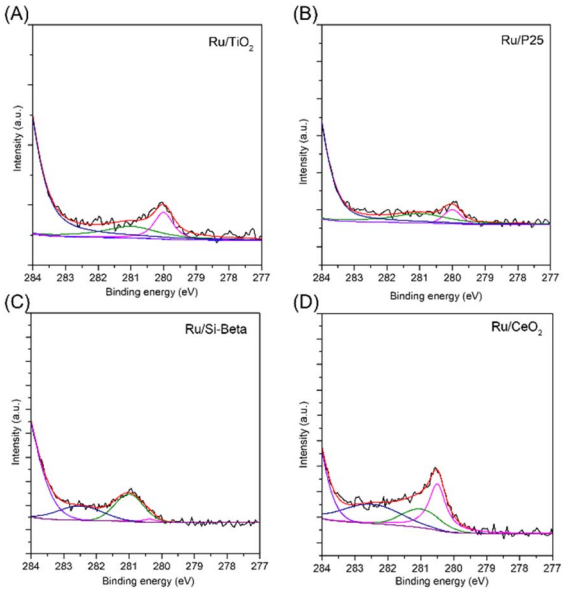

Fig. 3 Ru 3d XPS spectra of (A) Ru/TiO_2, (B) Ru/P25, (C) Ru/Si-beta and (D) Ru/CeO_2.

(PDF #82-1541), however, the peaks of RuO_2 probably overlaps with those of cordierite, and could not be identified directly.

X-ray photoelectron spectra (XPS) is employed to test various catalysts, and the high-resolution Ru 3d spectrum is displayed in Fig. 3. For Ru/TiO_2 and Ru/P25 catalysts, the Ru $3d_{5/2}$ can be deconvoluted into two peaks with binding energy at 281.0 eV and 280.0 eV, attributed to Ru^{4+} and Ru^0, corresponding to RuO_2 and metallic Ru nanoparticle, respectively.[18] Additionally, the binding energy of Ru^0 shifted to higher binding energy (280.5 eV) was observed in Ru/CeO_2 catalyst due to the electron transfer from Ru to Ce through Ce–O–Ru.[46] The Ru/CeO_2 catalyst showed one more Ru $3d_{5/2}$ peak with the binding energy at 282.5 eV, which can be assigned to Ru^{6+} species, probably resulting from the interaction between CeO_2 and Ru, thereby promoting the transformation of Ce^{4+} to Ce^{3+}, and causing the loss of electron of Ru.[47] For the Ti 2p spectra in Ru/TiO_2 and Ru/P25, two obvious peaks at 458.9 and 464.7 eV are in accordance with Ti $2p_{3/2}$ and Ti $2p_{1/2}$, indicating the Ti exsits in the form of Ti^{4+}.[48] For Ru/CeO_2 catalyst, the complicated Ce 3d spectra can be deconvoluted into eight components. The peaks located at 884.3 and 902.6 eV can be assigned to Ce^{3+} species, while the peaks at 882.1, 888.8, 898.1, 900.6, 907.5 and 916.5 eV are related to Ce^{4+} species (Fig. S3†).[49]

The temperature-programmed desorption of NH_3 (NH_3-TPD) experiments were conducted to examine the acidic properties of the as-obtained catalysts. As shown in Fig. 4, the peak that appears at a high temperature range of about 350–450 °C can be observed over Ru/TiO_2 and Ru/P25 catalyst, and corresponds to the strong acid sites.[50] In addition, the intensity of NH_3 desorption peak of Ru/TiO_2 catalyst is higher than those of Ru/P25, Ru/Si-beta and Ru/CeO_2 catalysts, indicating Ru/TiO_2 catalyst has abundant acid sites on its surface between 100 and 500 °C. Previous studies shows that the catalysts with abundant acid sites is beneficial for the adsorption of Cl and the cleavage

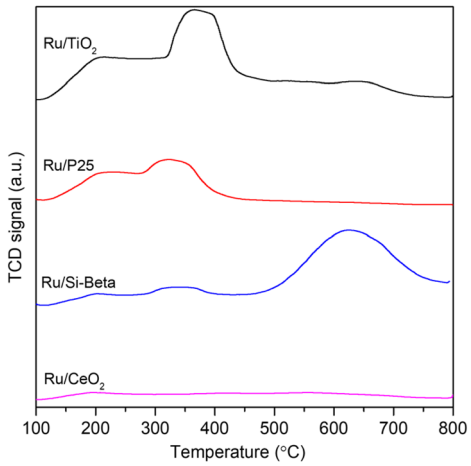

Fig. 4 The NH_3-TPD profiles of Ru/TiO_2, Ru/P25, Ru/Si-beta and Ru/CeO_2.

of C–Cl bonds during the DCM catalytic oxidation process.[49] In addition, the trend of surface acidity of various carriers is consistent with above catalysts within the same range of temperature (Fig. S4†).

The catalytic performance and CO_2 yield curves of prepared monolithic catalysts with various carriers for the DCM catalytic oxidation are displayed in Fig. 5. According to $T_{50\%}$ (reaction temperature of DCM conversion at 50%), the catalytic performance of the catalyst decreases in the order: Ru/TiO_2/Cor (329 °C) > TiO_2/Cor (351 °C) > Ru/P25/Cor (373 °C) > Ru/Si-beta/Cor (450 °C) > Ru/CeO_2/Cor (458 °C), and the Ru/TiO_2/Cor catalyst shows the superior catalytic activity in comparison with other samples, achieving almost 100% conversion of DCM at 400 °C, suggesting that the anatase TiO_2 as carrier is more favourable than others in improving the catalytic activity (Fig. 5A). This can be related to the surface acidity of Ru/TiO_2 which provides abundant acid sites for adsorption of Cl and the cleavage of C–Cl bonds. The DCM conversion over Ru/P25/Cor, Ru/Si-beta/Cor and Ru/CeO_2/Cor catalysts reached 94%, 55% and 52% at 460 °C, respectively. The CO_2 yield (Fig. 5B) of various catalysts follows similar trend as DCM conversion except for TiO_2/Cor catalyst. The TiO_2/Cor catalyst exhibits the worst CO_2 yield among the different catalysts because pure TiO_2 shows negligible activity over the cleavage of C–H bonds as well as CO oxidation (Fig. 5B). No surprisingly, the mineralization rate is elevated remarkably through the introduction of Ru onto the surface of TiO_2 nanoparticles. This can be related to the active Ru species with excellent redox capability, which is capable of oxidizing the intermediates effectively. Moreover, during the oxidation of DCM, TiO_2 will deactivate quickly owing to the adsorption and deposition of chlorine species onto its surface, and introducing Ru species will be more favorable in removing the chlorine species through the Deacon reaction, which eventually improving the catalytic performance. In addition, after the addition of Ru species on the surface of TiO_2 carrier, both the specific surface area and pore volume decreased slightly (Table 2), which may be caused by the fact that the Ru species enter into the channel of the carrier and block some pore during preparation process of Ru/TiO_2 powder catalyst.[35] Such results are also found in Ru/P25 and Ru/Si-beta catalysts. However, for Ru/CeO_2 catalyst, because the pore volume of CeO_2 is extremely low, the Ru species mainly deposited on the surface of CeO_2, as a consequence, causing a slight increase in specific surface area. The Ru/TiO_2/Cor catalyst shows the highest CO_2 yield of 97% at 460 °C, about 11%, 50% and 55% higher than those of Ru/P25/Cor, Ru/Si-beta/Cor and Ru/CeO_2/Cor catalysts, respectively. Carbon balance was also calculated over various catalysts at 460 °C based on the inlet and outlet results (Table S1†). For TiO_2/Cor catalyst, due to the weak oxidation capability of TiO_2, a large number of undesired by-products ($C_xH_yCl_z$) could be found in the outlet gas, and is much more than those of Ru/P25/Cor, Ru/Si-beta/Cor and Ru/CeO_2/Cor catalysts. For Ru/TiO_2/Cor

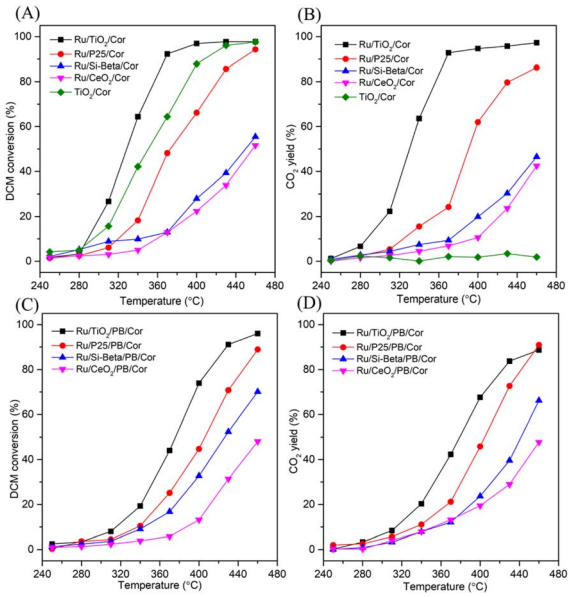

Fig. 5 (A) DCM conversion over Ru/TiO_2/Cor, Ru/P25/Cor, Ru/Si-beta/Cor, Ru/CeO_2/Cor and TiO_2/Cor catalysts; (B) CO_2 yield during DCM oxidation over Ru/TiO_2/Cor, Ru/P25/Cor, Ru/Si-beta/Cor, Ru/CeO_2/Cor and TiO_2/Cor catalysts; (C) DCM conversion over Ru/TiO_2/PB/Cor, Ru/P25/PB/Cor, Ru/Si-beta/PB/Cor and Ru/CeO_2/PB/Cor catalysts; (D) CO_2 yield during DCM oxidation over Ru/TiO_2/PB/Cor, Ru/P25/PB/Cor, Ru/Si-beta/PB/Cor and Ru/CeO_2/PB/Cor catalysts; 1000 ppm DCM, GHSV = 15 000 h^{-1}.

Table 2 Textural properties of the catalysts

Powder catalyst	S_{BET} ($m^2\ g^{-1}$)	Pore size (nm)	Pore volume ($cm^3\ g^{-1}$)
TiO_2	85.0	7.93	0.375
Ru/TiO_2	74.3	9.75	0.324
P25	51.4	17.67	0.219
Ru/P25	46.3	33.55	0.481
Si-beta	633.6	5.55	0.151
Ru/Si-beta	491.6	6.89	0.166
CeO_2	5.4	22.19	0.037
Ru/CeO_2	5.7	17.84	0.033

catalyst, based on the calculated result, negligible by-products ($C_xH_yCl_z$) could be existed in the outlet gas.

Moreover, the pseudo-boehmite sol used as binder was introduced into the preparation of monolithic catalysts to improve the adhesion between powder catalysts and cordierite honeycomb carrier. When the binder was introduced, the weight loss of coating on the Ru/TiO_2/PB/Cor catalyst is 6.5 wt%, and lower than that of Ru/TiO_2/Cor catalyst which is without binder (14.6 wt%) obviously. What's more, the light-off and CO_2 yield plots over the binder-containg monolithic catalysts are also recorded. As shown in Fig. 5C, the addition of pseudo-boehmite sol can result in change of catalytic activity of monolithic catalysts in different ways. For example, a temperature of 428 °C is needed to achieve 90% conversion of DCM over the Ru/TiO_2/PB/Cor catalyst, while the Ru/TiO_2/Cor catalyst only needs 368 °C to achieve the same conversion. The difference may result from the effect of binder. Pseudo-boehmite sol can be gradually transformed into Al_2O_3 during the calcination process. It has been reported that the Ru/Al_2O_3 shows lower catalytic performance toward DCM oxidation than that of Ru/TiO_2 because the TiO_2 carrier possesses the stronger Lewis acid sites compared to Al_2O_3, which is more active for the DCM dissociative adsorption.[34] Hence, introduction of pseudo-boehmite sol can restrict the catalytic behaviour of Ru/TiO_2/PB/Cor to some extent. Interestingly, the Ru/Si-beta/PB/Cor displays the contrary result by introducing the pseudo-boehmite sol in slurry. The $T_{50\%}$ for Ru/Si-beta/PB/Cor is 426 °C and lower than that of Ru/Si-beta/Cor (450 °C). The improved activity probably results from the Lewis acid sites that provided by Al_2O_3, which is considered to be favourable for DCM dissociative adsorption. Such result is different from the catalytic combustion of toluene that applying all-silicon beta zeolite supported Pd as catalysts. The authors found that the pure silica beta zeolite supported Pd catalyst with excellent hydrophobicity displayed highest catalytic activity for the catalytic oxidation of toluene than those catalysts with different SiO_2/Al_2O_3 ratio.[51] The DCM conversion over Ru/TiO_2/PB/Cor, Ru/P25/PB/Cor, Ru/Si-beta/PB/Cor and Ru/CeO_2/PB/Cor catalysts reached 96%, 89%, 70% and 48% at 460 °C, respectively. The CO_2 yield of Ru/TiO_2/PB/Cor (89%) is close to that of Ru/P25/PB/Cor (91%) at 460 °C, and about 23% and 41% higher than those of Ru/Si-beta/PB/Cor and Ru/CeO_2/PB/Cor catalysts. In addition, carbon balance results shows that the Ru/TiO_2/PB/Cor and Ru/Si-beta/PB/Cor produced little amounts of by-products ($C_xH_yCl_z$) at 460 °C. As shown in the Fig. 6A, the effect of different loading on catalytic activity of Ru/TiO_2/PB/Cor catalyst was also investigated. When the coating loading increased to about 13 wt%, the $T_{50\%}$ is 15 and 32 °C lower than those with loading of 8.5 wt% and 5.4 wt%, suggesting that the catalyst with higher loading is beneficial for the catalytic performance. Additionally, the influence of various GHSV over the Ru/TiO_2/PB/Cor catalyst toward DCM degradation was examined and displayed in Fig. 6B. When the GHSV is 15 000 h^{-1}, the $T_{50\%}$ and $T_{90\%}$ are 376 and 428 °C, about 26 and 31 °C higher than those under the 10 000 h^{-1}. Additionally, when the GHSV increased to 20 000 h^{-1}, a temperature of 447 °C is needed to achieve 90% conversion of DCM. Such results indicate that the Ru/TiO_2/PB/Cor catalyst showed ideal catalytic activity under various GHSV. Long-term

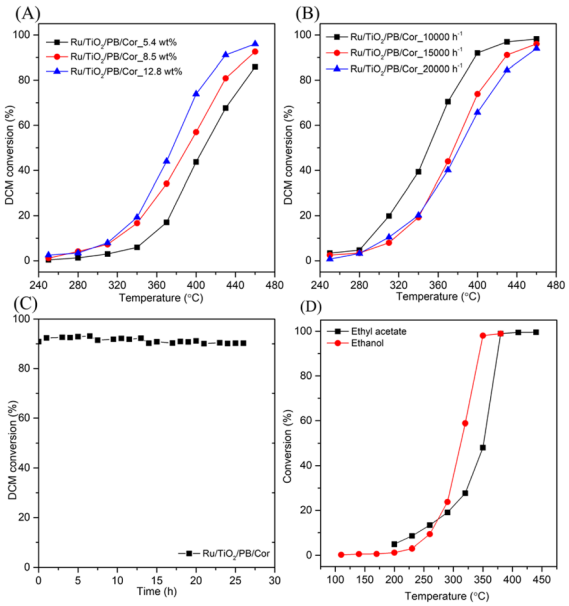

Fig. 6 (A) Effect of the loading over the Ru/TiO_2/PB/Cor catalyst; (B) effect of GHSV over the Ru/TiO_2/PB/Cor catalyst; (C) stability test of the Ru/TiO_2/PB/Cor catalyst for the degradation of DCM at 450 °C, 1000 ppm DCM, GHSV = 15 000 h^{-1}; (D) catalytic activity of ethyl acetate and ethanol over the Ru/TiO_2/PB/Cor catalyst; 1000 ppm EA; 1000 ppm EtOH; GHSV = 15 000 h^{-1}.

stability tests of Ru/TiO_2/PB/Cor catalyst at 450 °C was carried out and the result is displayed in Fig. 6C. It can be observed that the conversion of DCM over Ru/TiO_2/PB/Cor catalyst still can keep at ~90% even after 26 h, which suggests that the catalyst possesses excellent stability toward DCM catalytic oxidation. Such results can provide some valuable information for future pilot test or engineering applications. In addition, different types of VOCs, such as ethyl acetate and ethanol, are usually found to exist in industrial exhaust gas, thus, testing the adaptability of the as-obtained monolithic catalysts for the abatement of various VOCs is necessary. As shown in Fig. 6D, the $T_{90\%}$ for ethyl acetate and ethanol oxidation over Ru/TiO_2/PB/Cor catalyst is 375 °C and 344 °C, respectively, indicating that the catalyst is also applicable to the treatment of other VOCs.

Based on the published studies, only few have been reported to investigate the CVOCs catalytic oxidation over the monolithic catalysts with different catalytic active components during the past years. For example, Long *et al.* found that the optimized Mn–Ce–Zr monolithic catalyst displayed the best activity towards chlorobenzene (CB) oxidation with $T_{90\%}$ at 390 °C in comparison with other controlled samples.[15] Zhu *et al.* prepared a series of multi-structured Ag/MnO_2–cordierite molded catalysts that were applied in the catalytic oxidation of CB. The $T_{90\%}$ for EA and CB are 217 °C and 385 °C respectively under the space velocity of 10 000 h^{-1} over the optimized R–Ag/MnO_2–cordierite catalyst.[42] A higher temperature is usually needed to achieve the same conversion for CVOCs oxidation in comparison with other non-chlorine VOCs.

The DCM degradation mechanisms over various catalysts have been intensively studied and proposed. According to the

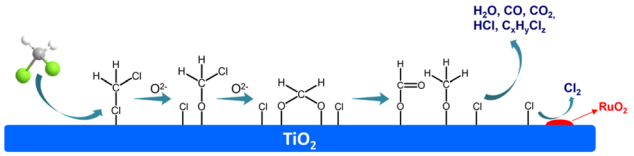

Fig. 7 Mechanism for the catalytic oxidation of DCM over the Ru/TiO_2/PB/Cor catalyst.

experiments and previous researches, the mechanism over Ru/TiO_2 monolithic catalyst can be deduced (Fig. 7): firstly, the DCM is adsorbed on the TiO_2 surface with abundant acidic sites, then attacked by surface active oxygen species adjacent to adsorbed DCM leading to the breakage of C–Cl bonds, and formed the chloromethoxy species.[49,52] In addition, the Cl of chloromethoxy species can also be adsorbed on the acidic sites, followed by the formation of bidentate methoxy species. Later the bidentate methoxy species can translate to formate species or the mixture of formate and formaldehyde species simultaneously.[49,53] Finally, the formate species can further be oxidized into CO or CO_2. At the same time, the dissociated adsorbed Cl species will be rapidly transferred to the Ru species, and followed by the generation of Cl_2 through Deacon reaction that catalyzed by RuO_2 component.[20,34,54]

4. Conclusion

In summary, a series of cordierite monolithic catalysts with Ru species supported on different low-cost available carriers were prepared and investigated for the degradation of CVOCs. Among them, the monolithic catalyst with Ru species supported on anatase TiO_2 carrier exhibited the desired catalytic activity for DCM oxidation with $T_{90\%}$ value of 368 °C. On the other hand, a pseudo-boehmite sol used as binder was introduced into the preparation of monolithic catalysts to further improve the adhesion between powder catalysts and cordierite honeycomb carrier. Although the $T_{50\%}$ and $T_{90\%}$ of the Ru/TiO_2/PB/Cor shifted to higher temperature of 376 and 428 °C, the weight loss of the coating for Ru/TiO_2/PB/Cor catalyst decreased to 6.5 wt%, which is significantly lower than that of Ru/TiO_2/Cor catalyst (14.6 wt%). In addition, the as-obtained Ru/TiO_2/PB/Cor catalyst also exhibited ideal catalytic property for the abatement of other VOCs. We believe that our work may provide new insights for design and development of high-performance catalysts through optimizing carriers and binders in a rational way to eliminate DCM as well as broaden its application to the degradation of non-chlorine VOCs.

Conflicts of interest

There are no conflicts to declare.

Acknowledgements

This work was supported by the National Key R&D Program of China (2022YFC3701600) and the preferential funding for Postdoctoral Research Projects of Zhejiang Province, China (ZJ2021052).

References

1 X. Zhang, Z. Pei, H. Lu and H. Huang, *RSC Adv.*, 2016, **6**, 84209–84215.
2 H. Huang, X. Zhang, X. Jiang, K. Dou, Z. Ni and H. Lu, *RSC Adv.*, 2016, **6**, 61610–61614.
3 X. Zhang, Z. Pei, X. Ning, H. Lu and H. Huang, *RSC Adv.*, 2015, **5**, 79192–79199.
4 C. Yang, G. Miao, Y. Pi, Q. Xia, J. Wu, Z. Li and J. Xiao, *Chem. Eng. J.*, 2019, **370**, 1128–1153.
5 L. Zhu, D. Shen and K. H. Luo, *J. Hazard. Mater.*, 2020, **389**, 122102.
6 Q. Dai, J. Wu, W. Deng, J. Hu, Q. Wu, L. Guo, W. Sun, W. Zhan and X. Wang, *Appl. Catal., B*, 2019, **249**, 9–18.
7 H. Liu, X. Li, Q. Dai, H. Zhao, G. Chai, Y. Guo, Y. Guo, L. Wang and W. Zhan, *Appl. Catal., B*, 2021, **282**, 119577.
8 J. M. Giraudon, T. B. Nguyen, G. Leclercq, S. Siffert, J. F. Lamonier, A. Aboukaïs, A. Vantomme and B. L. Su, *Catal. Today*, 2008, **137**, 379–384.
9 R. W. van den Brink, M. Krzan, M. M. R. Feijen-Jeurissen, R. Louw and P. Mulder, *Appl. Catal., B*, 2000, **24**, 255–264.
10 T. Cai, H. Huang, W. Deng, Q. Dai, W. Liu and X. Wang, *Appl. Catal., B*, 2015, **166–167**, 393–405.
11 S. Cao, H. Wang, M. Shi, S. Chen and Z. Wu, *Catal. Lett.*, 2016, **146**, 1591–1599.
12 W. Xingyi, K. Qian and L. Dao, *Appl. Catal., B*, 2009, **86**, 166–175.
13 P. Yang, S. Yang, Z. Shi, F. Tao, X. Guo and R. Zhou, *Chem. Eng. J.*, 2016, **285**, 544–553.
14 W. Deng, Q. Dai, Y. Lao, B. Shi and X. Wang, *Appl. Catal., B*, 2016, **181**, 848–861.
15 G. Long, M. Chen, Y. Li, J. Ding, R. Sun, Y. Zhou, X. Huang, G. Han and W. Zhao, *Chem. Eng. J.*, 2019, **360**, 964–973.
16 J. Chen, W. Xu, M. Jiang, J. Chen and H. Jia, *Appl. Catal., B*, 2020, **278**, 119263.
17 W. Sun, B. Gong, J. Pan, Y. Wang, H. Xia, H. Zhang, Q. Dai, L. Wang and X. Wang, *J. Catal.*, 2020, **391**, 132–144.
18 X. Liu, L. Chen, T. Zhu and R. Ning, *J. Hazard. Mater.*, 2019, **363**, 90–98.
19 S. Cao, X. Fei, Y. Wen, Z. Sun, H. Wang and Z. Wu, *Appl. Catal., A*, 2018, **550**, 20–27.
20 Y. Yang, H. Li, S. Zhang, X. Yu, S. Liu, R. Qu, C. Zheng and X. Gao, *Catal. Today*, 2020, **355**, 349–357.
21 Q. Dai, S. Bai, J. Wang, M. Li, X. Wang and G. Lu, *Appl. Catal., B*, 2013, **142–143**, 222–233.
22 I. Maupin, L. Pinard, J. Mijoin and P. Magnoux, *J. Catal.*, 2012, **291**, 104–109.
23 J. Zhao, W. Xi, C. Tu, Q. Dai and X. Wang, *Appl. Catal., B*, 2020, **263**, 118237.
24 Z. El Assal, S. Ojala, S. Pitkäaho, L. Pirault-Roy, B. Darif, J.-D. Comparot, M. Bensitel, R. L. Keiski and R. Brahmi, *Chem. Eng. J.*, 2017, **313**, 1010–1022.
25 L. Ran, Z. Wang and X. Wang, *Appl. Catal., A*, 2014, **470**, 442–450.

26 L. Ran, Z. Qin, Z. Wang, X. Wang and Q. Dai, *Catal. Commun.*, 2013, **37**, 5–8.
27 Q. Dai, S. Bai, X. Wang and G. Lu, *Appl. Catal., B*, 2013, **129**, 580–588.
28 Q. Dai, S. Bai, Z. Wang, X. Wang and G. Lu, *Appl. Catal., B*, 2012, **126**, 64–75.
29 R. López-Fonseca, B. de Rivas, J. I. Gutiérrez-Ortiz, A. Aranzabal and J. R. González-Velasco, *Appl. Catal., B*, 2003, **41**, 31–42.
30 X. Fei, S. Cao, W. Ouyang, Y. Wen, H. Wang and Z. Wu, *Chem. Eng. J.*, 2020, **387**, 123411.
31 Y. Shi, J. Wang, Y. Wang, F. Kong and R. Zhou, *J. Environ. Chem. Eng.*, 2022, **10**, 107629.
32 Q. Dai, W. Wang, X. Wang and G. Lu, *Appl. Catal., B*, 2017, **203**, 31–42.
33 Y. Su, K. Fu, Y. Zheng, N. Ji, C. Song, D. Ma, X. Lu, R. Han and Q. Liu, *Appl. Catal., B*, 2021, **288**, 119980.
34 Q. Ying, Y. Liu, H. Li, Y. Zhang and Z. Wu, *J. Colloid Interface Sci.*, 2022, **605**, 537–546.
35 X. Zhou, X. Lai, T. Lin, J. Feng, Z. Hou and Y. Chen, *New J. Chem.*, 2018, **42**, 16875–16885.
36 Q. Zhao, Y. Zheng, C. Song, Q. Liu, N. Ji, D. Ma and X. Lu, *Appl. Catal., B*, 2020, **265**, 118552.
37 M. Ma, R. Yang, Z. Jiang, C. Chen, Q. Liu, R. Albilali and C. He, *Fuel*, 2021, **303**, 121244.
38 V. Tomašić and F. Jović, *Appl. Catal., A*, 2006, **311**, 112–121.
39 M. L. Rodríguez, L. E. Cadús and D. O. Borio, *J. Environ. Chem. Eng.*, 2017, **5**, 292–302.
40 C. Hao, W. Huang, J. Zhang, J. Wu, Y. Yue and G. Qian, *J. Environ. Chem. Eng.*, 2021, **9**, 106145.
41 X. Lai, X. Zhou, H. Zhang, X. Jiang, T. Lin and Y. Chen, *Appl. Surf. Sci.*, 2020, **526**, 146714.
42 J. Zhu, W. Zhang, Q. Qi, H. Zhang, Y. Zhang, D. Sun and P. Liang, *Sci. Rep.*, 2019, **9**, 12162.
43 Z. Ren, V. Botu, S. Wang, Y. Meng, W. Song, Y. Guo, R. Ramprasad, S. L. Suib and P.-X. Gao, *Angew. Chem., Int. Ed.*, 2014, **53**, 7223–7227.
44 W. Zhao, Y. Dai, X. Cheng, S. Xu, Y. Guo and W. Fang, *Combust. Sci. Technol.*, 2021, **193**, 2009–2022.
45 C. Peng, T. Zhou, P. Wei, H. Ai, B. Zhou, H. Pan, W. Xu, J. Jia, K. Zhang, H. Wang and H. Yu, *Chem. Eng. J.*, 2022, **439**, 135685.
46 W. Liang, Y. Zhu, S. Ren, Q. Li, L. Song and X. Shi, *Appl. Catal., A*, 2021, **623**, 118257.
47 H. Huang, Q. Dai and X. Wang, *Appl. Catal., B*, 2014, **158-159**, 96–105.
48 D. Wang, J. Huang, F. Liu, X. Xu, X. Fang, J. Liu, Y. Xie and X. Wang, *Catal. Today*, 2020, **339**, 220–232.
49 S. Cao, H. Wang, F. Yu, M. Shi, S. Chen, X. Weng, Y. Liu and Z. Wu, *J. Colloid Interface Sci.*, 2016, **463**, 233–241.
50 J.-H. Jang, S.-C. Lee, D.-J. Kim, M. Kang and S.-J. Choung, *Appl. Catal., A*, 2005, **286**, 36–43.
51 Z. Zhang, L. Xu, Z. Wang, Y. Xu and Y. Chen, *J. Nat. Gas Chem.*, 2010, **19**, 417–421.
52 A. Khaleel and A. Al-Nayli, *Appl. Catal., B*, 2008, **80**, 176–184.
53 G. Busca, J. Lamotte, J. C. Lavalley and V. Lorenzelli, *J. Am. Chem. Soc.*, 1987, **109**, 5197–5202.
54 K. Seki, *Catal. Surv. Asia*, 2010, **14**, 168–175.